

BreastMultiNet: A multi-scale feature fusion method using deep neural network to detect breast cancer

Md. Mahbubur Rahman ^{a,b,*}, Md. Saikat Islam Khan ^{a,b,**}, Hafiz Md. Hasan Babu, Professor ^c

^a Department of Computer Science and Engineering, Mawlana Bhashani Science and Technology University, Bangladesh

^b Department of Computer Science and Engineering, Dhaka International University, Bangladesh

^c Department of Computer Science and Engineering, Dhaka University, Bangladesh

ARTICLE INFO

Keywords:

DenseNet-201

VGG19

Histogram oriented gradient

Local binary pattern

Speed-up robust feature

ABSTRACT

Breast cancer is predominantly seen in women and is the leading cause of death in females worldwide. Diagnosis of breast cancer using biopsy tissue images is expensive, time-intensive, and fraught with conflicts among doctors. Pathologists can now diagnose breast cancer more consistently and promptly because of advances in the Computer-Aided Diagnosis (CAD) system. As a result, there has been a surge in demand for CAD-based machine learning techniques. This study describes a “BreastMultiNet” framework that focuses on the transfer learning concept for identifying distinct types of breast cancer by utilizing two publicly available datasets. The suggested “BreastMultiNet” architecture allows rapid and comprehensive breast cancer diagnosis. The suggested scheme extracts features from microscope images with the help of well-known conventional and deep learning models such as HOG, LBP, SURP, DenseNet201, and VGG19. Comparatively, transfer learning models provide good accuracy than conventional models. The collected properties of transfer learning models are subsequently dispatched into the summing layer, resulting in a fused vector. The proposed framework achieves 99% and 95% classification accuracy on both BreakHis and ICIAR dataset respectively, outperforming all the other state of the art techniques. In terms of accuracy, the “BreastMultiNet” framework may be employed as a modeling approach in hospitals and medical care contexts.

1. Introduction

Breast cancer is the leading cause of cancer-related mortality in women in their early fifties worldwide. According to WHO, 2.3 million women are diagnosed with breast cancer in 2020, with 685,000 fatalities [1]. Breast cancer begins because of some breast cells are produced unnaturally [2]. Abnormal cells proliferate at a faster rate than normal tissues and continue to clump together to create lump. The cells have the potential to spread to the lymph nodes and other regions of the body [3]. Cells in the glandular tissue called lobules and many other tissues in the breast are the most prevalent causes of breast cancer [4,5]. Breast cancer may affect anybody, even males. According to estimates, 2650 males in the United States diagnosed with breast cancer in 2021, with around 530 dying [6]. If breast cancer is detected early, the survival rate will climb to 80%. Breast cancer detection methods often utilized include mammography, ultrasound, magnetic resonance imaging (MRI), and biopsy [7,8]. Breast abnormalities found by screening mammograms are

examined by radiologists [9]. Ultrasound may be employed to detect if a breast tumor is a solid mass or a liquid cyst, and MRI may locate deep damaged tissue [10]. Pigment and texture-based aspects of histopathological images are used to accomplish better segmentation activities [11]. Methods for histopathology imagery are fast advancing in medical image analysis, but an automated technique is still required to get efficient and economically accurate findings [12].

The most severe cancer is currently on the upswing due to the failure of diagnosing the disease early. Conventional and traditional machine learning methods are employed in a variety of medical issue domains [13,14]. Every year, many individuals die as a result of this cancer, and many people's lives are harmed as a result of it. The deep learning architecture was designed to address the disadvantages of previous approaches by automatically conducting the extraction operation in an entirely point-to-point path and learning the input images' comprehensive features from minimum to maximum levels for the classification strategy [15,16]. The suggested technique has developed a system that

* Corresponding author. Department of Computer Science and Engineering, Mawlana Bhashani Science and Technology University, Bangladesh.

** Corresponding author. Department of Computer Science and Engineering, Mawlana Bhashani Science and Technology University, Bangladesh.

E-mail addresses: mahbub.shimulbd@gmail.com (Md.M. Rahman), bappy.10.cse.mbstu@gmail.com (Md.S.I. Khan), hafizbabu@hotmail.com (H.Md.H. Babu).

detects breast cancer quickly and increases people's chances of survival. Proposed automated breast cancer identification structure named "BreastMultiNet" architecture. This system categorizes benign and malignant cancer from BreakHis images and invasive, benign, insitu, and normal breast cancer from ICIAR microscope images. We extract features from microscopy images using CNN pre-trained models and conventional models like VGG19, DenseNet-201, HOG, LBP, and SURF. In order to make the highest results, several feature extraction strategies were used in this study. Then, to aggregate all of the features, we utilized a concatenation layer with two best models. To get a fused vector, dense layers, normalizing layers, and dropout layers are employed in fine tuning. For classification, the last dense layer with the softmax function was used. The key contribution of this research is:

- In comparison to traditional machine learning methods, the "BreastMultiNet" framework enables clustering feature selection methods that do not need any manual extracting features procedures.
- The suggested framework performs well on benign data and does not misidentify any malignant data.
- The performance of the "BreastMultiNet" framework is examined on both huge and small samples. The results show that our system is capable of obtaining great performance in both scenarios.

The entire technique is divided into the following sections: Section 2 discusses prior work on breast cancer, as well as the suggested "BreastMultiNet" architecture and data augmentation technique discussed in Sections 3 and 4 show the findings and experimental setup. Section 5 discusses comparative research and future directions. With the conclusion, Section 6 is revealed.

2. Literature review

It is challenging to identify and classify breast cancer using deep neural networks. A large number of researchers have utilized various methodologies or strategies in the identification of breast cancer. Some modern techniques to breast cancer detection are mentioned in this section. According to the literature lesson, breast cancer detection approaches are classified into three categories: image preparation, extraction of features, and classification.

Zhang et al. suggested a multi-scale residual convolutional neural network (MSRCNN) and SVM-based autodiscovery approach with IDC. Before feeding the patches from whole slide images (WSI) into the MSRCNN for feature extraction, they were preprocessed using data augmentation and normalization. Then, the gathered features were sent into the SVM, which classified them as either good or affected patches. The experimental result shows an accuracy level of 87.45% throughout five times cross-validation [17]. Celik, Y., et al. (2020) suggested an automated identification of invasive ductal carcinoma (IDC), the most frequent form of breast cancer, with a deep machine learning approach. They employed deep learning pre-trained models, ResNet-50 and DenseNet-161, in their research to identify IDC. In their experiments, they used a public histopathology dataset including 277,524 image slices. DenseNet-161 model has a normalized accuracy value of 91.57% as a consequence of learning on the final tiers of pre-trained deep learning framework [18]. Furthermore Xiangyu Song et al. developed bi-graph contrastive learning-based knowledge tracing employing two-layer structural sections based on four real-world datasets [48]. To construct discriminative interpretation of tasks and ideas, RNN and memory-augmented neural networks are used at the node level and graph level, respectively. The proposed technique generates accurate visualizations and projected results through concurrent constructive loss. N. Aristokli et al. (2022) examined different breast cancer detection strategies. MRI was already claimed to disclose new evidence among them. Mammography, ultrasonography and MRI evaluate performance in diagnosing breast cancer based on the type of tumor, breast density, and patient history. MRI has the highest sensitivity 94.6% as a

standalone modality, while mammography has the lowest sensitivity independent of breast shape, densities, or histories [8]. In another research, a variational co-embedding trained model for associated system groupings embedded with nodes and attributes was suggested by Yang, S. et al. on the basis of four genuine attributed network datasets [49]. A reciprocal distance loss on the Gaussian priors' centers improves functionality..Ibrahim et al. developed a CNN architecture with 15 fully connected layers and two entirely connected layers compared with six distinct activation functions. The dataset used, PatchCamelyon, has 220, 000 classified images for train and 57,000 unclassified test images. In this investigation, the formed measure achieved the highest AUC value, 95.46% [19]. V. Gupta et al. (2021) suggested a revised residual neural network-oriented technique detecting breast cancer histopathological images. Suggested technique performs well at illumination levels of 40X, 100X, 200X, and 400X. On the BreakHis dataset with a scale factor of 40X, the network achieves an average accuracy of classification 99.75% [20]. Moreover In order to directly understand the underlying characteristics and relationships between tweets, social ties, and the publishing time, Yin, H. et al. introduced an end-to-end deep learning approach called DFMF (Deep Fusion of Multimodal Features) [50]. To understand the high-level meanings of tweets and the underlying abstractions of the intricate social links, the proposed fusion uses a word embedding layer and a node embedding layer, respectively. In comparison to LR and SVM, the suggested DFMF performs better in forecasting the retweet time, achieving up to 11.25% performance. After that in order to filter the noisy elements for cross-network node classification using two real-world graph datasets as samples, Yang, S. et al. present a robust graph domain adaptive learning framework called RGDAL [51]. For the estimate of mutual information, the approach is constructed using a dynamic neighborhood sampling technique that can discretize the graph and include graph spatial features. Lastly, compared to SOTA graph adaptive learning approaches, it demonstrates superior resilience for cross-network node categorization. In another study, Agaba, A. J., et al. (2022) used custom extracting features approaches and Deep Neural Network for breast cancer identification on the publicly available BreakHis data. The findings show that utilizing customized feature extractors technique and DNN classifiers had a superior accuracy of 97.87% for 40x magnifications in breast cancer multi-classification [21]. Brancati recommends a deep neural strategy for recognizing IDC and categorizing lymphoma subclasses in breast histology images. They employed intrinsic CNN in all cases and contrasted CNN with the UNet and ResNet designs. They proposed an approach based on Intrinsic CNN and a softmax classification function to tackle the two circumstances that bypass custom pathological characteristics. The proposed method eventually achieved a 97.06% accuracy [22]. Melekoodappattu, J. G., et al. (2022) developed an integration technique for independent cancer diagnosis that used a nine-layer modified convolutional neural network. Texture characteristics and their proportions are lowered using Uniform Manifold Approximation and Projection to increase classification efficacy in the extraction-based stage. A proposed clustering was used to aggregate the findings of each step to arrive at a conclusion, which had 98% accuracy [23]. Roy et al. developed a patch-oriented classifier that uses CNN in two ways: first, one patch one decision, and second, all patches one decision. They utilized the 2018 ICIAR breast histological imaging collection, divided into four subgroups: normal, benign, insitu, and invasive cancer. Their overall rate of success is 87% [24]. Furthermore on the basis of seven well-known short text datasets, Yin, H. et al. offer two ways to make use of the unsupervised autoencoder (AE) framework based on these pre-trained text models for the best clustering performance [52]. In the suggested technique, they employ Graph Convolutional Networks as encoders to combine the structural characteristics with those of the Structural Text Network Graph Autoencoder (STN-GAE) to build text networks. They used a different technique called Soft Cluster Assignment Autoencoder to make the learnt text representations more clustering-friendly. Dey S. et al. (2022) established an automated breast cancer diagnosis method that receives thermal

breast images and utilizes the DenseNet121 framework as a feature extractor. The Database for Mastology Research (DMR-IR) breast imaging dataset was utilized to assess the efficiency of their system, and it attained the maximum classification accuracy of 98.80% [25].

3. Proposed methodology

This section shows how to use several multi-scale transfer learning models to identify breast images. The suggested “BreastMultiNet” structure employed in this identification is depicted in Fig. 1. Various preprocessing approaches are used before dividing the dataset into training, testing and validation class. Following that, a comprehensive data augmentation approach expands the dataset magnitude. Proposed architecture holds the retrieving features from expanded features. Lastly, the proposed research trained the system using the two publicly available datasets separately, then utilizing the testing images to evaluate the proposed “BreastMultiNet” architecture. The subsequent sections provide details on the blocks linked to the proposed architecture.

3.1. Dataset

The proposed “BreastMultiNet” architecture in breast cancer diagnosis is evaluated using two currently accessible data in this research. BreakHis data is one of them [26]. Another source of data is ICIAR data [27]. BreakHis dataset combines benign and malignant cancer patients, with 2480 and 5429 patients, respectively. Four benign tumours are depicted in the benign microscopic images: adenoma, phyllodes, fibroadenoma, and adenosis. Tumours in the malignant data include carcinoma, lobular, mucinous, and papillary. The microscopic data were acquired from 82 patients using several magnification factors, namely 400X, 200X, 100X, and 40X. All of the microscope images were chosen patient-by-patient rather than image-by-image. Datasets are collected from diverse patients to increase dispatch unmatching and improve validity. ICIAR 2018 dataset contains 400 hematoxylin and eosin-stained microscopic images of breast histopathology. The ICIAR data is categorized as follows: normal, insitu, benign, and invasive cancer, with each category including 100 images of mammary. Fig. 2 shows a selected group of images derived from the BreakHis and ICIAR

collection. Table 1 contains supplemental facts on both datasets.

3.2. Data preprocessing stage

Many preprocessing techniques were employed before putting the images into the fine-tuned variational deep learning approach, as illustrated in Fig. 3. The BreakHis data consists all micro images in png format, having 3-channels of RGB and an 8-bit resolution for each channel. We converted a huge number of high-resolution images to 224×224 pixels using machine learning algorithms. The suggested method converts gathered images into Numpy arrays, allowing the model to train more quickly and less storage. The complete dataset is broken down into three sections. 30% of the data was utilized for testing and validation, while the remaining was used for training. The overfitting problem is addressed to make the model more robust, and several data augmentation procedures are also utilized [28]. After using the data preprocessing approach, the size of this dataset has grown from 7909 to 54,403. Zooming is performed with parameter value two, rotation with 90° angle, shearing with 0.5 value, 0.4 width and height shifted value is used in preprocessing stage. After that vertical and horizontal flipping is applied to adequate expanded features. In the ICIAR dataset, All tiff format images are converted into the desired format and resized 224×224 pixels using the transfer learning principle. Following that, the research has applied the same procedure with the BreakHis collection to enhance the performance accuracy. The image count in the ICIAR dataset increased to 2560 from 400 after applying the data augmentation technique. Table 2 displays the cancer type-wise dataset applying the data augmentation technique.

3.3. Constructing multiple-scale feature learning model

By merging VGG19 with DenseNet201, we suggested a unique multi-scale neural adapting system in this study. The hybrid model captures low-level properties before constructing a multiple-scale feature learning process to evaluate these features at various scales. Propose BreastMultiNet fine tuning process is illustrated in Fig. 3. Integrated characteristics include microscopic image sharpening, blurring, texturing, and gradients alignment [29]. After merging all of the

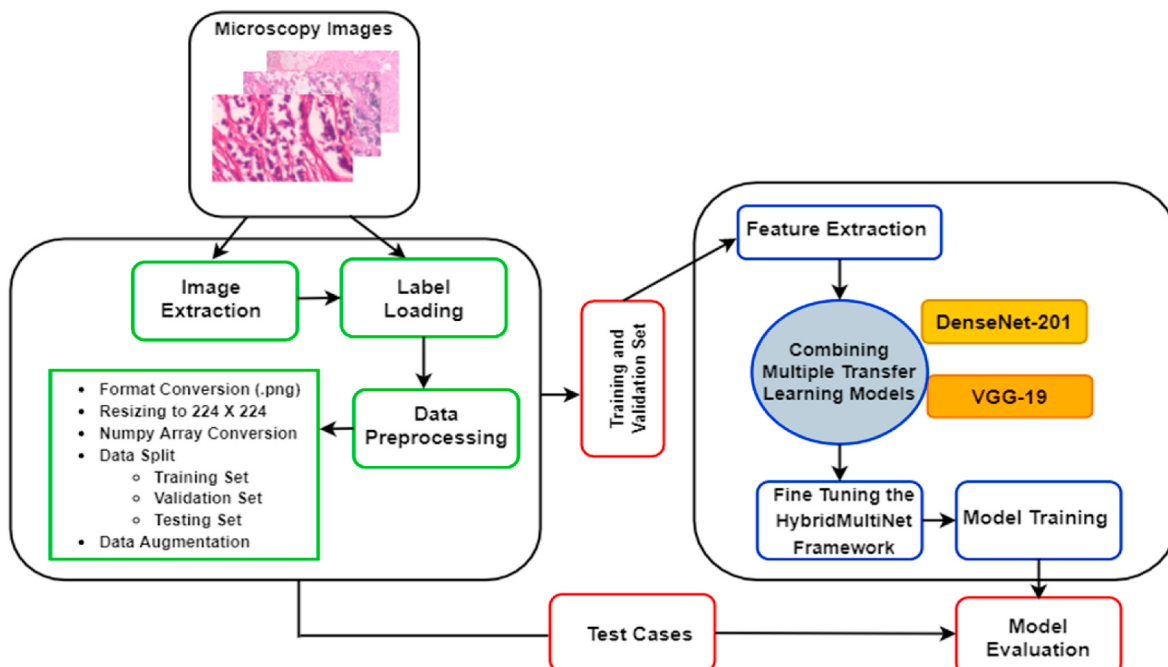


Fig. 1. Basic diagram of breast cancer classification.

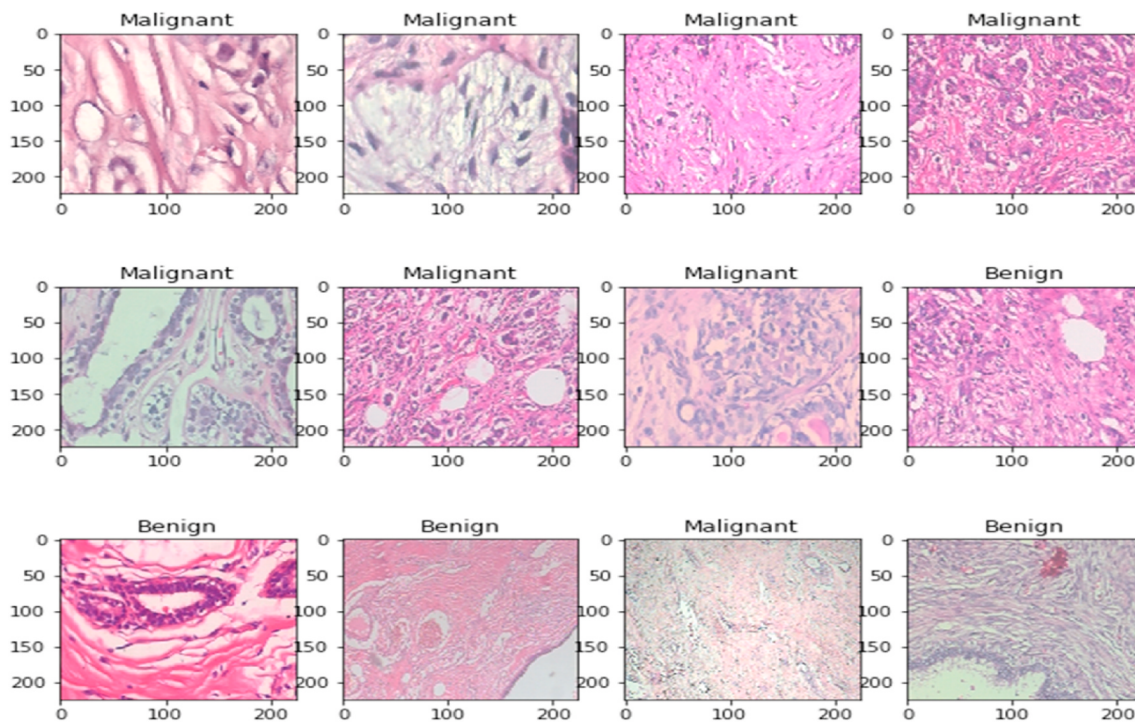


Fig. 2. Derived sample images from both datasets.

Table 1

Cancer type-wise dataset before data augmentation.

Cancer Type	BreakHis Dataset			ICIAR Dataset		
	Train	Validate	Test	Train	Validate	Test
Benign Cancer	1924	481	75			
Malignant Cancer	4274	1070	85			
Normal				70	20	10
Insitu				70	20	10
Benign				70	20	10
Invasive				70	20	10

Table 2

Cancer type-wise dataset after data augmentation.

Cancer Type	BreakHis Dataset			ICIAR Dataset		
	Train	Validate	Test	Train	Validate	Test
Benign Cancer	13,468	3367	75			
Malignant Cancer	29,918	7490	85			
Invasive				490	140	10
Normal				490	140	10
Insitu				490	140	10
Benign				490	140	10

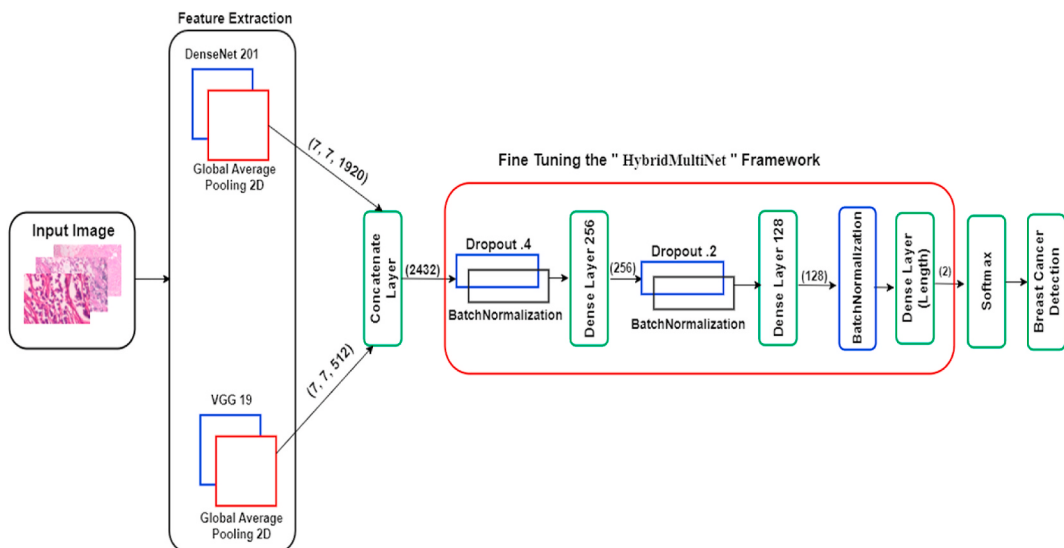


Fig. 3. Fine Tuning Process of "BreastMultiNet" framwork.

characteristics, the suggested “BreastMultiNet” framework contains 39,013,634 parameters, which are 3, 9, and 3 times more than the separate DenseNet201 and VGG19 designs. The form and content of each accepted CNN pre-trained system, as well as the fine-tuning approaches, are covered in the following sub-sections.

3.3.1. Visual geometry group network (VGG19)

In the 2014 ILSVRC competition, Simonyan et al. produced the VGGNet pre-trained model, winning first place in image translation and second place in image classification [30]. When compared to the AlexNet design, the VGGNet architecture performed admirably, with an error rate of 8.1%. The convolution layer is divided into 5 layers. In each successive max-pooling tier, the employment of a ReLU function as a non-linear kernel function assures that the output of each fully-connected layer is more powerful. The depths of the next five levels are 64, 128, 256, 512, and 512, in that order. Every tier is separated into subregions, each of which uses max-pooling to decrease the trainable parameters. The last layer was a critical rule in obtaining the feature vector of the recommended VGG19 models [31]. The details illustration of VGG19 based CNN architecture is given in Fig. 4.

3.3.2. Dense convolutional networks (DenseNet201)

Huang et al. created the DenseNet pre-trained model, which has the highest accuracy on the CIFAR10, CIFAR-100, and ImageNet datasets in 2017 [32]. This concept evolved into such a ResNet concept, in which the feed from one layer is relayed to the other layers in a precise way. This link allows the network to communicate essential information inside the model, resulting in more effective network training and enhanced network performance [33]. As an initial component extractor, the system used the DenseNet201 pre-trained model. DenseNet201 layers outperform with a limited dataset by tackling overfitting complications while performing. Furthermore, by overcoming the gradient descent problem, the DenseNet201 model significantly improves the ImageNet database [34]. When deeper CNN tiers are integrated with DenseNet, the DenseNet201 pre-trained model performed more detailed than the AlexNet, ResNet, and GoogLeNet design [35,36].

3.3.3. Histogram oriented gradient (HOG)

HOG, a feature extraction technique, was applied in this study. The input image is first converted to grayscale before being turned into a gradient image for better edge recognition. Every signal unit collects the

slope or edges orientation histogram, which is subsequently mixed to provide a HOG descriptor [37,38]. A slope in both the x and y axis must be created before the feature can be extracted in HOG. The following idioms depict the HOG architecture. $I(x, y)$ represent the pixel intensities of x and y , and g_x represents the orientation slope of x , whereas g_y represents the orientation slope of y (x, y). The slope magnitude of x and y is denoted by $g(x, y)$ and estimated by

$$g_x = I(x+1, y) - I(x-1, y) \quad (1)$$

$$g_y = I(x, y+1) - I(x, y-1) \quad (2)$$

$$\Delta g(x, y) = \sqrt{(g_x^2 + g_y^2)} \quad (3)$$

and the gradient direction of x and y is calculated by

$$\theta = \arctan \left(\frac{g_y}{g_x} \right) \quad (4)$$

3.3.4. Local binary pattern (LBP)

The surface and regional spatial analysis of ultrasound images are explored by LBP [39]. A threshold value, expressed by 0 and 1, is utilized to level the adjacent pixels. Each surrounding pixel gray value (3×3) is leveled as 1 if it is greater than the central pixel value; else, it is ground as 0. Accordingly, The LBP is a set of binary values that substitute the converted to the decimal mean pixel value. In equation (5) and (6); P stands for pixel intensity, g_p the i th neighboring pixel, and g_c the center pixel. The acquired LBP code is used to extract the histogram characteristics of size 2^P . As a result, the histogram feature vector length for 8 surrounding pixels is 256.

$$l = \sum_{p=0}^{P-1} S(g_p - g_c) 2^p \quad (5)$$

$$S = \begin{cases} 1; & \text{if } (i,j) > 0 \\ 0; & \text{otherwise} \end{cases} \quad (6)$$

3.3.5. Speed-up robust feature (SURF)

SURF is a representational and comparing approach that is independent by resemblance. In nearest neighbor screening, SURF uses its robust features extraction approach [40]. SURF is capable of extracting

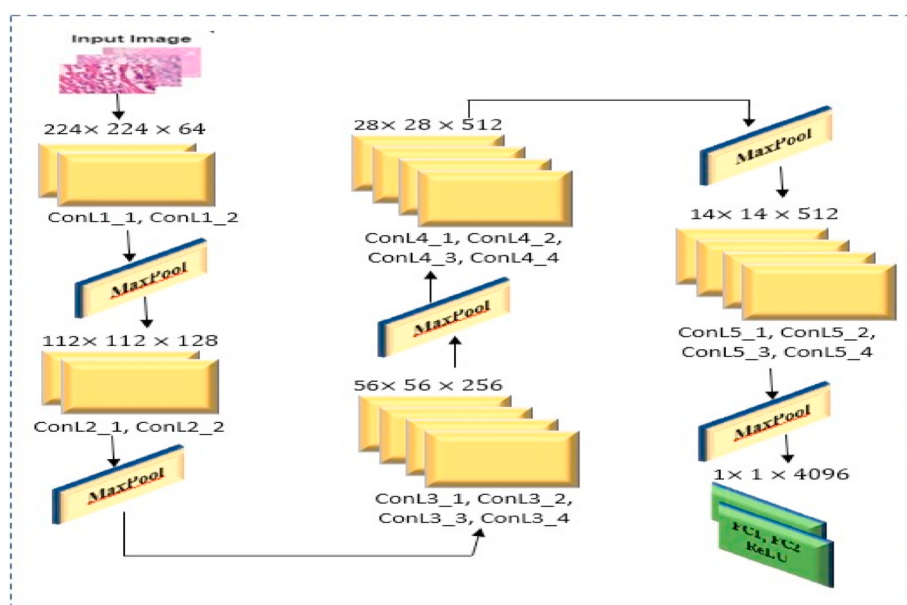


Fig. 4. VGG19 based CNN architecture.

attributes during augmentation. Box filtering is used by SURF, a scaling and rotation variation approach, to facilitate rapid operator calculation [41]. SURF has two functions: feature extraction and feature description. The Hessian matrix assumption is used in SURF to extract features. The SURF identifier gives each detail on the features formed by the surroundings around an object of interest. SURF works by employing Haar wavelet responses to indicate the specific orientation of an interesting point. The neighboring interest regions are flipped to the desired direction before computing the descriptor. Formula (7) provides the Hessian matrix $H(x, \sigma)$. The wavelet response in the horizontal and vertical directions is represented in Equation (8) by dx and dy , respectively. For each segment, a vector V is measured.

$$H(\dot{x}, \sigma) = \begin{bmatrix} L_{xx}(x, \sigma) & L_{xy}(x, \sigma) \\ L_{xy}(x, \sigma) & L_{yy}(x, \sigma) \end{bmatrix} \quad (7)$$

$$V = \left\{ \sum dx, \sum dy, \sum |dx|, \sum |dy| \right\} \quad (8)$$

3.4. Fine tuning process

Fig. 3 demonstrates the use of distinct, fully linked tiers to integrate several transfer learning approaches for identifying breast carcinoma classifications. Continuing the extraction of each characteristic one by one, all of the pre-trained models utilize GlobalAveragePooling2D to flatten all of the layers into a vector by finding the average value for each of the input channels. Using the concatenate layer, all of the distinct vectors are concatenated into a single vector. Following that, six layers are employed to fine-tune the combined features for our classification job, accompanied by a SoftMax activation function. Overfitting is a severe problem in the deep learning model that happens whenever the system over-trains on training examples, resulting in unsatisfactory test results [42]. We employ two dropout layers to overcome the overfitting problem. The very first dropping tier will discard most of the sample during model training, whereas the subsequent dropout tier will eliminate less sample than the previous tier.

Furthermore, thus an approach considerably facilitates the training phase's acceleration. In addition, two batch normalization layers are used in our classification model, which is critical. The batch normalization layer will reorganize all of the data to normalize it quickly. The reorganized data will aid in the acceleration of the training process while also reducing vulnerability to system startup. A density tier is a wholly linked tier that contains most of the neurons from the prior and current levels. These tiers process the input data and produce a result. This final layer will calculate the probability based on the length of the expected class. The SoftMax activation function analyzes the outcome

chances and decides which attributes are most associated with the specific predicted class. In the SoftMax procedure, the result value is between 0 and 1, prompting the neuron to fire. The given equation SoftMax function is defined:

$$\text{softmax}(z)_j = \frac{\exp(z_j)}{\sum_{k=1}^l \exp(x_k)} \quad (9)$$

The results of combining diverse deep learning methods and ultimately linked tiers are shown in Table 3. The statistic was generated during working on the boolean segmentation technique. As a result, there are two units in the ultimate entirely linked tier. However, while dealing with ICIAR data, we use four units in the final deep network. The suggested "BreastMultiNet" module's other architecture is similar to deployed with a categorization algorithm. A proposed algorithm for our "BreastMultiNet" architecture is presented below, with each stage of the process outlined.

The proposed "BreastMultiNet" framework for detecting breast cancer cases given as Algorithm 1.

Algorithm 1

Automated breast cancer detection and classification from histopathology images.

```

Input: Histopathology images Training set δ1, Validation set δ2, and Testing set δ3.
      a ← Learning rate.
      b ← Epochs.
      c ← Batch size.
      n ← The number of images covered in one batch size.
Output: w← "Histopathology" framework weight.
begin:
  1. Convert each Histopathology image in training set into 224 × 224.
  2. Perform data augmentation strategy for increasing the dataset size.
  3. Extract the features from the Histopathology images using DenseNet-201 and
     VGG-19 CNN pre-trained models.
  4. Combine the extracted features using the concatenate layer.
  5. Set the fine-tuned layers  $\text{CNN}_{\text{dense}}$ ,  $\text{CNN}_{\text{batchnormalization}}$ ,  $\text{CNN}_{\text{dropout}}$ , and  $\text{CNN}_{\text{softmax}}$ .
  6. Initialize the CNN pre-trained model parameters: a, b, c, n.
  7. Train the "BreastMultiNet" framework and determine the initial weights.
  8. for b = 1 to b do
    9. Select a mini batch size (size: n) for training set δ1.
    10. Forward propagation and determine the loss function.
    11. Backpropagation and update the weight w.
  12. end for

```

4. experimental design and results computation

The discovered architecture, hyper-parameters utilized in the research, and findings obtained from the BreakHis and ICIAR datasets

Table 3

The details of the proposed "BreastMultiNet" framework.

Layer (type)	Parameter	Result Formation	Linked with
input_1 (InputLayer)	0	(None, 224, 224, 3)	
Densenet201 (Functional)	18,321,984	(None, 7, 7, 1920)	input_1[0][0]
vgg19 (Functional)	20,024,384	(None, 7, 7, 512)	input_1[0][0]
global_average_pooling2d (Global)	0	(None, 1920)	Densenet201[0][0]
global_average_pooling2d_2 (Global)	0	(None, 512)	vgg19[0][0]
concatenate (Concatenate)	0	(None, 2432)	global_average_pooling2d[0][0]
global_average_pooling2d_1 (Global)			global_average_pooling2d_1[0][0]
dropout (Dropout)	0	(None, 2432)	concatenate[0][0]
batch_normalization (BatchNormalization)	9728	(None, 2432)	dropout [0][0]
dense (Dense)	622,848	(None, 256)	batch_normalization[0][0]
dropout_1 (Dropout)	0	(None, 256)	dense [0][0]
batch_normalization_1 (BatchNormalization)	1024	(None, 256)	dropout_1[0][0]
dense_1 (Dense)	32,896	(None, 128)	batch_normalization_1[0][0]
batch_normalization_2 (BatchNormalization)	512	(None, 128)	dense_1[0][0]
dense_2 (Dense)	258	(None, 2)	batch_normalization_2[0][0]
Total parameters: 39,013,634			
Trainable params: 38,778,946			
Non-trainable params: 234,688			

using the “BreastMultiNet” architecture are shown in this section. A detailed comparison of the proposed approach and the particular CNN model is shown in Fig. 4.

4.1. Experimental design

The suggested “BreastMultiNet” architecture was built utilizing Keras, an open-source package that connects Python to neural networks. On a 64-bit Windows 11-based pc, we train and evaluate the model using Jupyter Notebook (PC). The computer comes with 8 GB of RAM and a 2.80 GHz Intel 11th Generation Core i7 CPU.

4.2. Performance metrics

Several quantitative measures such as Precision, Recall, False-positive rate, True negative rate (TNR), F1-Score, and Matthews correlation coefficient (MCC) are used to evaluate the efficacy of the proposed framework. Such parameters as True Positive (TP), True Negative (TN), False Positive (FP), and False Negative (FN) are dependent on the conclusion of the confusion matrix. The term “TP” refers to a result in which the suggested “BreastMultiNet” framework accurately detected the positive breast cancer kind. The term “TN” indicates a result in which the suggested scheme accurately identified the kind of breast cancer that is negative. The term FP denotes a situation in which the proposed framework misidentified positive breast. The term “FN” describes a situation in which the proposed framework misidentified the type of negative tumours. The following are the names of all evaluation metrics:

$$\text{Accuracy} = \frac{TP + TN}{TP + TN + FP + FN} \quad (10)$$

$$\text{Sensitivity} = \frac{TP}{TP + FN} \quad (11)$$

$$\text{Specificity} = \frac{TN}{TN + FP} \quad (12)$$

$$\text{Precision} = \frac{TP}{TP + FP} \quad (13)$$

$$\text{F1-score} = 2 \times \frac{Pr \times Re}{Pr + Re} \quad (14)$$

$$\text{MCC} = \frac{TP \times TN - FP \times FN}{\sqrt{(TP + FP)(TP + FN)(TN + FP)(TN + FN)}} \quad (15)$$

4.3. Training and parameter optimization

Fig. 5 depicts the simulation outcome for the BreakHis dataset while training the proposed “BreastMultiNet” architecture. The error unit of slope descent and the optimization equation are two important hyperparameters to consider while training a model [43]. We chose adam variable employed as the optimization equation because it connects important values of various optimizers capable of handling sparse gradients on big datasets. Because our BreakHis dataset has binary features, we used binary cross-entropy as a loss function. We require an ideal learning rate value to reduce the loss function. We chose a learning rate of 0.0001 in this experiment. Furthermore, a modest batch size of 32 was utilized, demonstrating appropriate generalization of the system. The suggested approach was acquainted on the 25th epoch. However, after just the 19th epoch of training, the model achieved more than 99% training accuracy and 98% validation accuracy. The overfitting problem is also absent during the training phase, as seen in Fig. 5 (a). Fig. 5 (b) shows how the arc drastically reduces the loss percentage.

Fig. 6 shows the accuracy progression and loss when training the recommended “BreastMultiNet” architecture on the ICIAR collection. We utilized cross-entropy as a gradient descent because our study is focused on multi-label categorization in the ICIAR sample. The suggested approach needed to be developed with more features due to the restricted number of images in this dataset. The “BreastMultiNet” architecture trained for 245th epochs and obtained 97% training accuracy just after the 180th epoch. As a result, the cumulative validation accuracy throughout the validation stage is 97%. Fig. 6(b) demonstrates the error function graph, which shows that the loss value is near to 0 and that no fluctuations occur throughout training and validation. Fig. 6(a) further shows that the overfitting problem is not apparent.

4.4. Result discussions

The confusion table and ROC graph for the BreakHis sample utilizing the “BreastMultiNet” architecture are shown in Fig. 7. The suggested system merged two well-known transfer learning approaches, DenseNet201 and VGG19, and then used the fusion characteristics to determine whether breast tissue is benign or cancerous. Fig. 7(a) indicates that most of the images are correctly labeled as benign and malignant breast carcinoma, with only one misclassification. Simultaneously, the suggested approach misclassifies just one benign microscopic image. The region score for this design is 0.998, suggesting that the model is consistent and reliable. In addition, various deep learning techniques are tested independently on the BreakHis data better to understand the usefulness of the “BreastMultiNet” architecture. Table 4 shows a comparison of the “BreastMultiNet” architecture and the other five transfer learning models. The “BreastMultiNet” architecture exceeds all existing

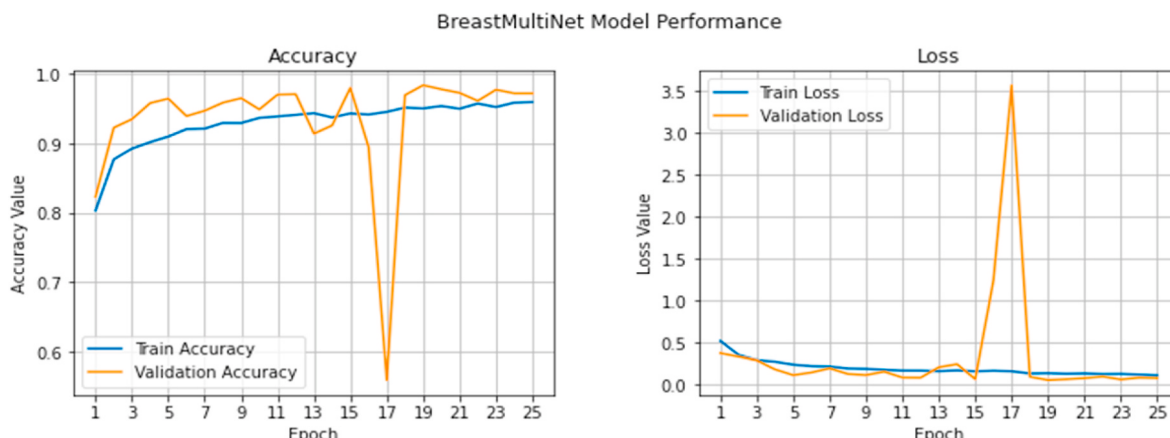


Fig. 5. BreakHis data during training and validation: (a) Epoch vs Accuracy Value. (b) Epoch vs Loss Value.

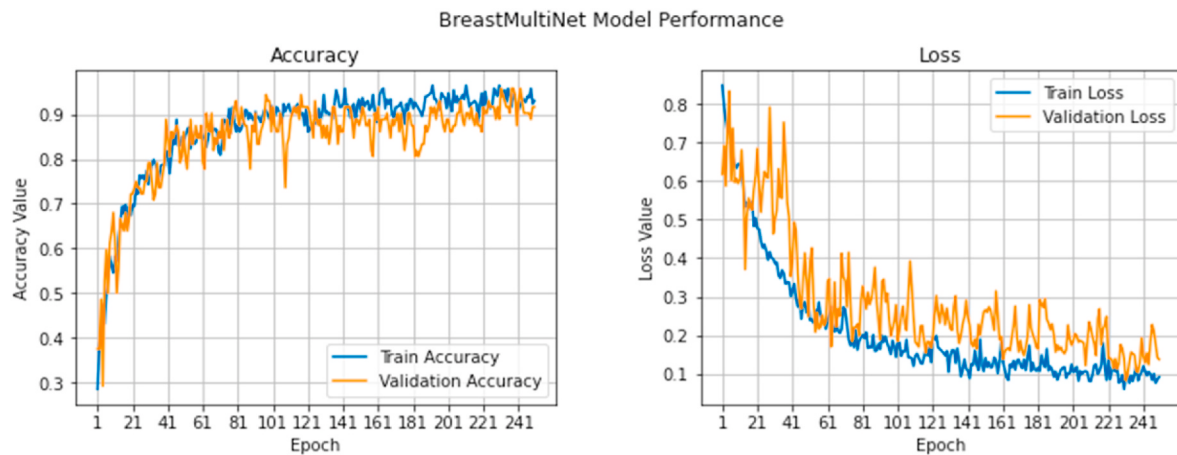


Fig. 6. ICIAR data during training and validation: (a) Epoch vs Accuracy Value. (b) Epoch vs Loss Value.

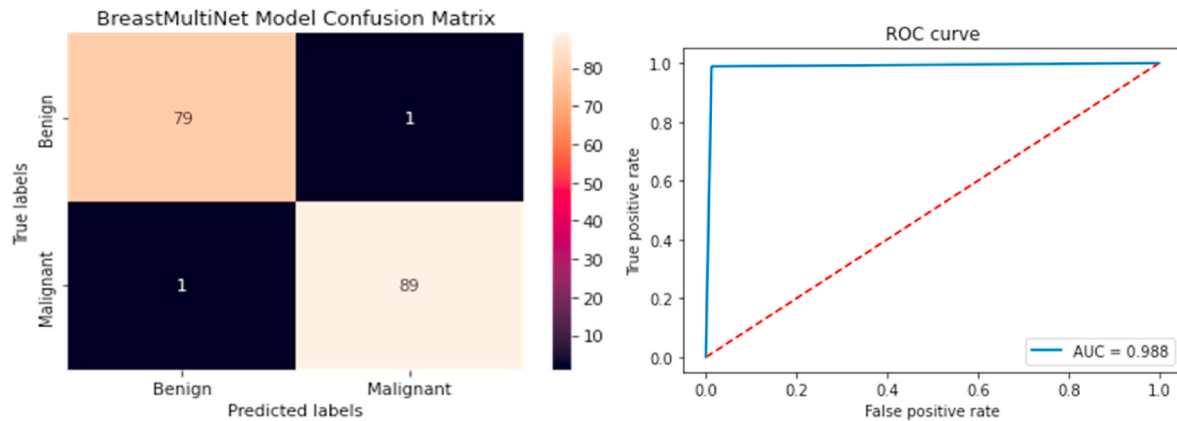


Fig. 7. BreakHis dataset: (a) Confusion matrix. (b) ROC.

Table 4

A comparison study of five learning models and “BreastMultiNet” method on BreakHis Dataset.

Methods	Cancer Type	TP	TN	FP	FN	Precision	Recall	FPR	TNR	F1-score	MCC
DensNet201	Benign	72	81	4	3	0.946	0.956	0.045	0.945	0.950	0.905
	Malignant	81	72	3	4	0.958	0.945	0.039	0.956	0.957	0.907
	Average Score					0.945	0.945	0.035	0.956	0.952	0.906
VGG16	Benign	71	77	8	4	0.901	0.951	0.089	0.912	0.923	0.854
	Malignant	77	71	4	8	0.954	0.912	0.051	0.952	0.931	0.851
	Average Score					0.917	0.925	0.065	0.926	0.925	0.846
VGG19	Benign	69	81	4	6	0.946	0.916	0.039	0.956	0.931	0.874
	Malignant	81	69	6	4	0.926	0.951	0.081	0.920	0.936	0.867
	Average Score					0.935	0.935	0.055	0.936	0.935	0.866
MobileNet	Benign	40	77	8	35	0.828	0.531	0.088	0.959	0.656	0.484
	Malignant	77	40	35	8	0.693	0.911	0.456	0.538	0.788	0.479
	Average Score					0.756	0.716	0.277	0.716	0.725	0.486
ResNet-50	Benign	47	81	4	28	0.919	0.625	0.049	0.953	0.749	0.613
	Malignant	81	47	28	4	0.735	0.951	0.369	0.328	0.842	0.624
	Average Score					0.825	0.786	0.206	0.790	0.800	0.621
Proposed method	Benign	79	89	1	1	0.988	0.988	0.011	0.989	0.989	0.977
	Malignant	89	79	1	1	0.989	0.989	0.012	0.988	0.994	0.990
	Average Score					0.989	0.989	0.011	0.989	0.992	0.984

state-of-the-art models with an average accuracy of 0.997, recall of 0.997, f1-score of 0.995, and MCC of .993. The FNR is 0.010, and the TNR is close to one, showing that the model is effective. The DenseNet201 performed well, with a f1-score and TNR value of 0.952 and 0.956, respectively.

Using the “BreastMultiNet” architecture, Fig. 8 depicts the confusion sequence and Roc area for the ICIAR sample. The conceptual approach

detects the multiclass carcinoma group in this dataset, encompassing benign, InSitu, invasive, and normal. Fig. 8(a) demonstrates the proper categorization of 10, 8, 10, and 10 microscopic images as four different types of multiple cancers. The “BreastMultiNet” framework, on the other hand, misclassifies just one benign microscopic image. This paradigm has an area score of 0.935, showing that the model is consistent and comprehensive. Table 5 additionally includes a comparison study,

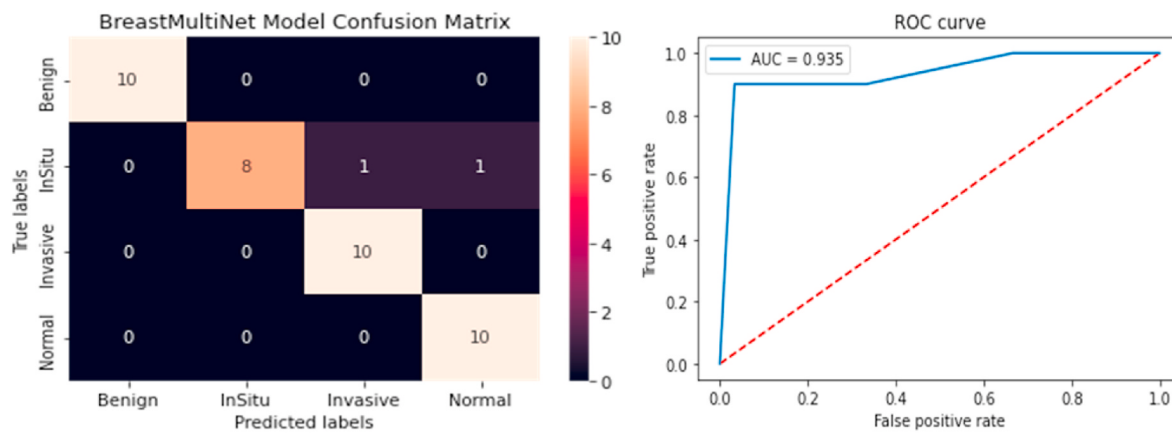


Fig. 8. ICIAR data: (a) Confusion matrix. (b) ROC.

Table 5

A comparison study of five learning models and “BreastMultiNet” method on ICIAR Dataset.

Model	Cancer Type	TP	TN	FP	FN	Precision	Recall	FPR	TNR	F1-Score	MCC
DensNet201	Benign Cancer	10	28	2	0	0.831	1.000	0.055	0.945	0.910	0.881
	InSitu Cancer	8	30	0	2	1.000	0.803	0.000	1.000	0.894	0.872
	Normal Cancer	8	29	1	2	0.892	0.802	0.029	0.968	0.842	0.794
	Invasive Cancer	9	28	2	1	0.817	0.902	0.056	0.938	0.856	0.812
	Average Score					0.880	0.868	0.037	0.958	0.880	0.841
VGG16	Benign Cancer	7	28	2	3	0.778	0.704	0.068	0.934	0.742	0.658
	InSitu Cancer	8	25	5	2	0.0624	0.801	0.168	0.834	0.703	0.593
	Normal Cancer	5	30	0	5	1.000	0.500	0.000	1.000	0.674	0.654
	Invasive Cancer	8	25	5	2	0.621	0.801	0.167	0.826	0.701	0.594
	Average Score					0.754	0.702	0.100	0.900	0.699	0.618
VGG19	Benign Cancer	7	25	5	3	0.584	0.703	0.156	0.835	0.635	0.503
	InSitu Cancer	4	29	1	6	0.802	0.396	0.026	0.971	0.526	0.484
	Normal Cancer	9	25	5	1	0.636	0.901	0.162	0.843	0.746	0.666
	Invasive Cancer	6	27	3	4	0.674	0.601	0.102	0.904	0.631	0.526
	Average Score					0.674	0.654	0.446	0.554	0.654	0.541
MobileNet	Benign Cancer	0	29	1	0	0.001	0.001	0.024	0.959	0.002	0.001
	InSitu Cancer	5	20	10	5	0.331	0.501	0.334	0.674	0.401	0.154
	Normal Cancer	2	29	1	8	0.670	0.201	0.026	0.968	0.312	0.269
	Invasive Cancer	8	17	13	2	0.384	0.801	0.429	0.571	0.521	0.321
	Average Score					0.351	0.384	0.210	0.791	0.379	0.156
ResNet-50	Benign Cancer	7	28	2	3	0.784	0.701	0.067	0.931	0.739	0.659
	InSitu Cancer	8	26	4	2	0.666	0.801	0.129	0.874	0.732	0.631
	Normal Cancer	9	29	1	1	0.901	0.898	0.026	0.968	0.901	0.869
	Invasive Cancer	8	29	1	2	0.890	0.799	0.023	0.971	0.838	0.791
	Average Score					0.841	0.801	0.068	0.928	0.801	0.741
Proposed method	Benign Cancer	10	30	0	0	1.000	1.000	0.000	1.000	1.000	1.000
	InSitu Cancer	8	30	0	2	1.000	0.800	0.000	1.000	0.890	0.870
	Normal Cancer	10	29	1	0	0.910	1.000	0.033	0.970	0.953	0.940
	Invasive Cancer	10	29	1	0	0.910	1.000	0.033	0.970	0.953	0.940
	Average Score					0.960	0.950	0.017	0.990	0.952	0.941

which reveals that the “BreastMultiNet” architecture obtains an average accuracy of 0.995, recall of 0.996, f1-score of 0.991, and MCC of 0.981. Table 5 further shows that the conceptual approach outperformed the other five models in terms of detecting breast cancer subtypes. The DenseNet-201 and ResNet50 pre-trained models attain more than 70% classification accuracy among the five-transfer deep learning. The other three models, on the other hand, underperform in classifying the multiple breast cancer group.

Individual performance values for many traditional feature extraction approaches such as HOG, LBP, and SURF are less than sufficient. Only DensNet201 outperforms other approaches on both datasets, with accuracy ranging from 50% to 60%. Table 6 eventually shown that the suggested fused structure outperforms all existing methods.

5. Result analysis

This “BreastMultiNet” architecture presents a technique for BreakHis

Table 6

The results of the conventional models and the suggested model are compared.

Models	Dataset	Accuracy	Specificity	Sensitivity
HOG	BreakHis	0.566	0.675	0.702
	ICCIAR	0.661	0.714	0.783
SURF	BreakHis	0.657	0.643	0.740
	ICCIAR	0.487	0.567	0.514
LBP	BreakHis	0.634	0.710	0.793
	ICCIAR	0.871	0.786	0.887
VGG19	BreakHis	0.933	0.921	0.873
	ICCIAR	0.675	0.654	0.710
DensNet201	BreakHis	0.945	0.953	0.925
	ICCIAR	0.886	0.861	0.901
Proposed (VGG19+DensNet201)	BreakHis	0.992	0.989	0.989
	ICCIAR	0.952	0.960	0.950

Table 7

Comparison among existing methods and proposed “BreastMultiNet” model.

Authors	Classification Class	Methodology	Accuracy
Saini et al. (2020) [46]	Multiclass	DCGAN and VGG16	94.5%
Alzubaidi et al. (2020) [47]	Multiclass	Hybrid CNN	96.1%
Zhang et al. (2021) [17]	Binary Class	MSRCNN and SVM	87.45%
Celik et al. (2020) [18]	Binary Class s	ResNet50 and DensNet161	91.57%
Ibrahem et al.(2020) [19]	Multiclass	Modified CNN	95.46%
Gupta et al. (2021) [20]	Binary Class	MRNN	99.75%
Agaba et al.(2021) [21]	Binary Class	DNN	97.87%
Brancati et al.(2019) [22]	Binary Class	Residual CNN	97.06%
Melekodappattu et al. (2022) [23]	Multiclass	Modified CNN	98%
Roy et al. (2019) [24]	Multiclass	CNN	87%
Dey et al. (2022) [25]	Multiclass	DensNet201	98.80%
Proposed Method	Binary Class	DensNet201, VGG19, and Fine-tune	99.2%
Proposed Method	Multiclass	DensNet201, VGG19, and Fine-tune	95.2%

and ICIAR breast cancer data using microscope images. Table 7 compares the “BreastMultiNet” framework’s performance to that of previous studies that employed identical datasets but with various patterns, features, as well as depth sizes. Table 7 reveals that, compared to previous studies, the suggested method has the greatest prediction accuracy in both malignant and benign classification and benign, inSitu, invasive, and normal cancer detection. We achieved an average classification accuracy of 99% for the BreakHis dataset and 98% for the ICIAR dataset by effectively blending all pretrained approaches. Fig. 9 illustrates several of the microscope images that the framework anticipates. Moreover, there are notable benefits to employing this method beyond the previous techniques outlined in the previous studies. Prior research employed a variety of features extraction methodologies, which are sometimes ineffective when working with a huge dataset [44,45]. Celik et al. employed two well-known pre-trained breast cancer histology image models, ResNet50 and DensNet161. His experiment dataset had

277,524 patches, which is insufficient for obtaining acceptable accuracy [18]. Although most of the authors put in significant exertion to train a system, unsatisfactory outcomes were acquired behind experimenting with various designs [17,24,46]. Alzubaidi et al. proposed a new CNN architecture with more than 70 layers for multigroup breast cancer classification in another research [47]. In the binary dataset, Saini and Susan (2020) addressed the data difficulty. DCGAN was exclusively used to improve results from minority populations. If DCGAN training were applied to all data sets, the distribution would be unable to generalize [46]. Our suggested technique, on the other hand, does not misidentify any hazardous images in the BreakHis or ICIAR datasets. When compared to state-of-the-art methodologies, our built system achieved the greatest classification performance and is ready to be tested with more diversified large databases.

6. Conclusions

This paper presents a revolutionary deep “BreastMultiNet” model for more accurately and consistently detecting breast cancer patients from microscope images. It entails running a number of independent pre-trained Convolutional networks in simultaneously before combining them to form a single model for each organs or organ’s categorization assignment. The system was utilized and validated on a variety of image data, both huge and small. It is constructed in such a way that it can function efficiently on a wide range of datasets. Experiment findings show that the “BreastMultiNet” framework outperforms both separate CNN pre-trained architectures, achieving 99% classification accuracy in the BreakHis data and 95% classification accuracy ICIAR data, respectively. Furthermore, it has a good performance in recognizing cancerous images, boosting the chances of survival. Based on these positive results, we feel that our “BreastMultiNet” model would become an excellent option for assisting doctors in quickly diagnosing and detecting breast cancer.

Author contribution

MMR designed the study. SIK, and MMR wrote the manuscript; SIK collected data. HSB, MMR, and SIK edited the manuscript; MMR, and

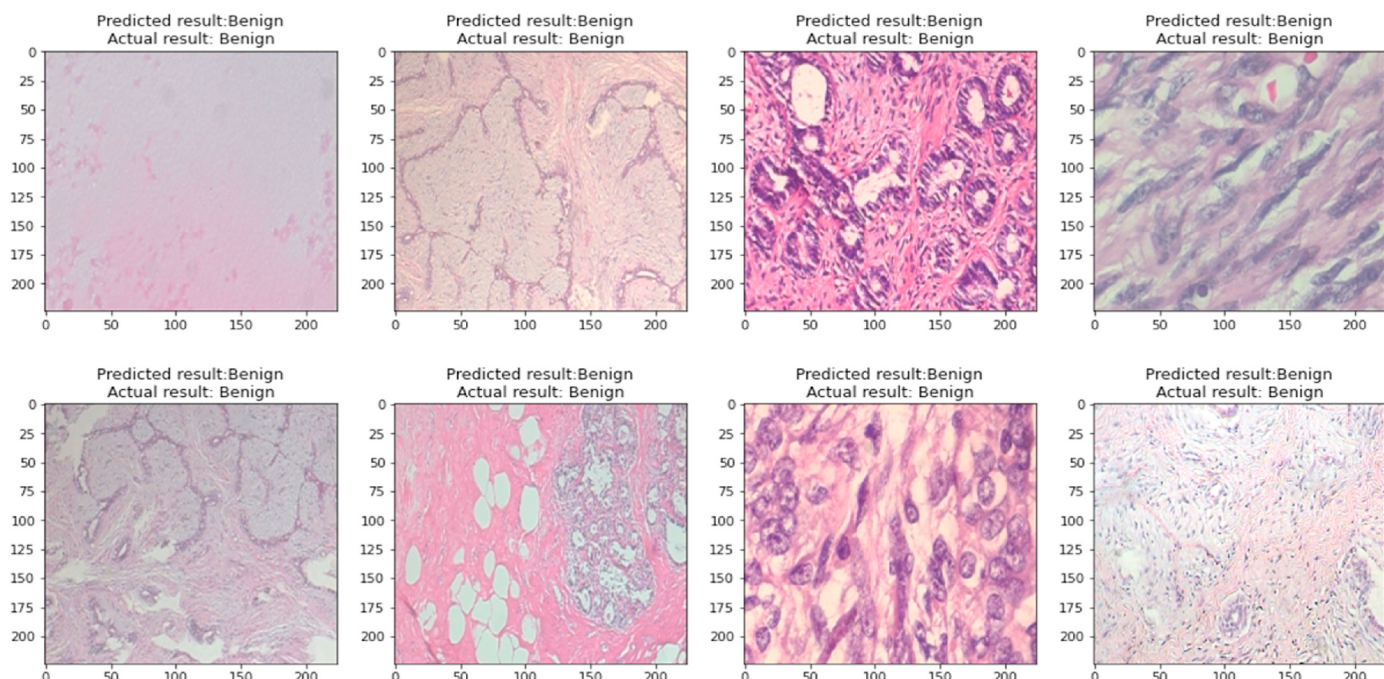


Fig. 9. Predicted microscopy images using “BreastMultiNet” framework.

SIK performed the analyses. SIK, and MMR generated all figures and tables. All of the authors have read and approved the final version of the paper.

Declaration of competing interest

The authors declare no competing financial/non-financial interests.

Data availability

Data will be made available on request.

References

- [1] Sung H, et al. Global cancer statistics 2020: GLOBOCAN estimates of incidence and mortality worldwide for 36 cancers in 185 countries. *CA A Cancer J Clin* 2021;71(3):209–49.
- [2] Yu J, et al. Challenges and opportunities in metastatic breast cancer treatments: nano-drug combinations delivered preferentially to metastatic cells may enhance therapeutic response. *Pharmacol Therapeut* 2022;108108.
- [3] Kalot R, Mhanna R, Talhouk R. Organ-on-a-chip platforms as novel advancements for studying heterogeneity, metastasis, and drug efficacy in breast cancer. *Pharmacol Therapeut* 2022;108156.
- [4] Raja GB. Early detection of breast cancer using efficient image processing algorithms and prediagnostic techniques: a detailed approach. In: *Cognitive systems and signal processing in image processing*. Elsevier; 2022. p. 223–51.
- [5] Unal YC, et al. The role of connexins in breast cancer: from misregulated cell communication to aberrant intracellular signaling. *Tissue Barr* 2022;10(1):1962698.
- [6] Siegel RL, et al. Cancer statistics, 2022. *CA: Cancer J Clinic* 2022.
- [7] Hernández L, et al. Magnetic resonance imaging in diagnosis of indeterminate breast (BIRADS 3 & 4A) in a general population. *Insights Imag* 2021;12(1):1–17.
- [8] Aristokli N, et al. Comparison of the diagnostic performance of Magnetic Resonance Imaging (MRI), ultrasound and mammography for detection of breast cancer based on tumor type, breast density and patient's history: a review. *Radiography* 2022;28(3):848–56.
- [9] Geertse TD, et al. Added value of prereding screening mammograms for breast cancer by radiologic technologists on early screening outcomes. *Radiology* 2022;302(2):276–83.
- [10] Prabha K, et al. Different diagnostic aids and the improved scope of establishing early breast cancer diagnosis. In: *Micro-electronics and telecommunication engineering*. Springer; 2021. p. 65–72.
- [11] Alzubaidi L, et al. Novel transfer learning approach for medical imaging with limited labeled data. *Cancers* 2021;13(7):1590.
- [12] Wang J, et al. A review of deep learning on medical image analysis. *Mobile Network Appl* 2021;26(1):351–80.
- [13] Shamshirband S, et al. A review on deep learning approaches in healthcare systems: taxonomies, challenges, and open issues. *J Biomed Inf* 2021;113:103627.
- [14] Rahman MM, et al. Hybrid feature fusion and machine learning approaches for melanoma skin cancer detection. 2022.
- [15] Caroppi A, Leone A, Siciliano P. Deep transfer learning approaches for bleeding detection in endoscopy images. *Comput Med Imag Graph* 2021;88:101852.
- [16] Liu X, et al. A review of deep-learning-based medical image segmentation methods. *Sustainability* 2021;13(3):1224.
- [17] Zhang J, et al. Automatic detection of invasive ductal carcinoma based on the fusion of multi-scale residual convolutional neural network and SVM. *IEEE Access* 2021;9:40308–17.
- [18] Celik Y, et al. Automated invasive ductal carcinoma detection based using deep transfer learning with whole-slide images. *Pattern Recogn Lett* 2020;133:232–9.
- [19] Kandel I, Castelli M. A novel architecture to classify histopathology images using convolutional neural networks. *Appl Sci* 2020;10(8): 2929.
- [20] Gupta V, et al. Breast cancer detection from histopathology images using modified residual neural networks. *Biocybern Biomed Eng* 2021;41(4):1272–87.
- [21] Agaba AJ, et al. Improved multi-classification of breast cancer histopathological images using handcrafted features and deep neural network (dense layer). *Intell Syst Appl* 2022;200066.
- [22] Brancati N, et al. A deep learning approach for breast invasive ductal carcinoma detection and lymphoma multi-classification in histological images. *IEEE Access* 2019;7:44709–20.
- [23] Melekodappattu JG, et al. Breast cancer detection in mammogram: combining modified CNN and texture feature based approach. *J Ambient Intell Hum Comput* 2022;1:10.
- [24] Roy K, et al. Patch-based system for classification of breast histology images using deep learning. *Comput Med Imag Graph* 2019;71:90–103.
- [25] Dey S, et al. Screening of breast cancer from thermogram images by edge detection aided deep transfer learning model. *Multimed Tool Appl* 2022;1:19.
- [26] Spanhol FA, et al. A dataset for breast cancer histopathological image classification. *IEEE Trans Biomed Eng* 2015;63(7):1455–62.
- [27] Aresta G, et al. Bach: grand challenge on breast cancer histology images. *Med Image Anal* 2019;56:122–39.
- [28] Nugroho K, Noersasongko E. Enhanced Indonesian ethnic speaker recognition using data augmentation deep neural network. *J King Saud Univ-Comput Informat Sci* 2021;34(7):4375–84.
- [29] Karim R, Shahriar A, Rahman MM. Machine learning-based tri-stage classification of Alzheimer's progressive neurodegenerative disease using PCA and mRMR administered textural, orientational, and spatial features. *Int J Imag Syst Technol* 2021;31(4):2060–74.
- [30] Simonyan K, Zisserman A. Very deep convolutional networks for large-scale image recognition. 2014. arXiv preprint arXiv:1409.1556.
- [31] Akhtar N, Ragavendran U. Interpretation of intelligence in CNN-pooling processes: a methodological survey. *Neural Comput Appl* 2020;32(3):879–98.
- [32] Huang G, et al. Densely connected convolutional networks. In: *Proceedings of the IEEE conference on computer vision and pattern recognition*; 2017.
- [33] Hao W, Zhang Z. Spatiotemporal distilled dense-connectivity network for video action recognition. *Pattern Recogn* 2019;92:13–24.
- [34] Luminii A, Nanni L. Deep learning and transfer learning features for plankton classification. *Ecol Inf* 2019;51:33–43.
- [35] Alqudah A, Alqudah AM. Sliding window based deep ensemble system for breast cancer classification. *J Med Eng Technol* 2021;45(4):313–23.
- [36] Luz DS, et al. Automatic detection metastasis in breast histopathological images based on ensemble learning and color adjustment. *Biomed Signal Process Control* 2022;75:103564.
- [37] Hussein IJ, et al. Fully-automatic identification of gynaecological abnormality using a new adaptive frequency filter and histogram of oriented gradients (HOG). *Expet Syst* 2021;e12789.
- [38] Li Y, et al. Research on invasive species recognition based on SVM+ HOG. In: *2021 2nd international conference on artificial intelligence and information systems*; 2021.
- [39] Kushwaha R, Singal G, Nain N. A texture feature based approach for person verification using footprint bio-metric. *Artif Intel Rev* 2021;54(2):1581–611.
- [40] Hoque MZ, et al. Whole slide image registration via multi-stained feature matching. *Comput Biol Med* 2022;105301.
- [41] Bakheet S, Al-Hamadi A, Youssef R. A fingerprint-based verification framework using harris and SURF feature detection algorithms. *Appl Sci* 2022;12(4):2028.
- [42] Shetty SP, et al. Thermo-hydraulic performance prediction of a solar air heater with circular perforated absorber plate using Artificial Neural Network. *Therm Sci Eng Prog* 2021;23:100886.
- [43] Victoria AH, Maragatham G. Automatic tuning of hyperparameters using Bayesian optimization. *Evolv Syst* 2021;12(1):217–23.
- [44] Adadi A. A survey on data-efficient algorithms in big data era. *J Big Data* 2021;8(1):1–54.
- [45] Collaboration SI. Machine learning and health care disparities in dermatology. 2018.
- [46] Saini M, Susan S. Deep transfer with minority data augmentation for imbalanced breast cancer dataset. *Appl Soft Comput* 2020;97:106759.
- [47] Alzubaidi L, et al. Optimizing the performance of breast cancer classification by employing the same domain transfer learning from hybrid deep convolutional neural network model. *Electronics* 2020;9(3):445.
- [48] Song Xiangyu, Li Jianxin, Qi Lei, Zhao Wei, Chen Yunliang, Mian Ajmal. Bi-CLKT: Bi-graph contrastive learning based knowledge tracing. *Knowl Base Syst* 2022;241:108274. <https://doi.org/10.1016/j.knosys.2022.108274>. ISSN 0950-7051.
- [49] Yang S, Verma S, Cai B, Jiang J, Yu K, Chen F, Yu S. Variational Co embedding learning for attributed network clustering. 2021. arXiv preprint arXiv:2104.07295.
- [50] Yin H, Yang S, Song X, Liu W, Li J. Deep fusion of multimodal features for social media retweet time prediction. *World Wide Web* 2021;24(4):1027–44.
- [51] Yang S, Cai B, Cai T, Song X, Jiang J, Li B, Li J. Robust cross-network node classification via constrained graph mutual information. *Knowl Base Syst* 2022;257:109852.
- [52] Yin H, Song X, Yang S, Huang G, Li J. Representation learning for short text clustering. In: *International conference on web information systems engineering*. Cham: Springer; 2021, October. p. 321–35.